AIP | Review of Scientific Instruments

Operando x-ray photoelectron emission microscopy for studying forward and reverse biased silicon p-n junctions

N. Barrett, D. M. Gottlob, C. Mathieu, C. Lubin, J. Passicousset, O. Renault, and E. Martinez

Citation: Review of Scientific Instruments **87**, 053703 (2016); doi: 10.1063/1.4948597
View online: http://dx.doi.org/10.1063/1.4948597
View Table of Contents: http://scitation.aip.org/content/aip/journal/rsi/87/5?ver=pdfcov
Published by the AIP Publishing

Articles you may be interested in

Towards monomaterial p-n junctions: Single-step fabrication of tin oxide films and their non-destructive characterisation by angle-dependent X-ray photoelectron spectroscopy
Appl. Phys. Lett. **107**, 231601 (2015); 10.1063/1.4937003

Opto-electronic modeling of light emission from avalanche-mode silicon p+n junctions
J. Appl. Phys. **118**, 114506 (2015); 10.1063/1.4931056

Photoemission induced bias in two-dimensional silicon pn junctions
Appl. Phys. Lett. **99**, 202107 (2011); 10.1063/1.3662440

Studies of W(100) modified by praseodymium oxide by using x-ray photoelectron spectroscopy, low-energy electron diffraction, and photoelectron emission microscopy
J. Vac. Sci. Technol. B **27**, 698 (2009); 10.1116/1.3070656

Pulsed laser ultrahigh vacuum deposited silicon in the presence of excess cesium and oxygen studied with x-ray photoelectron spectroscopy and atomic force microscopy
J. Vac. Sci. Technol. A **21**, 874 (2003); 10.1116/1.1577137

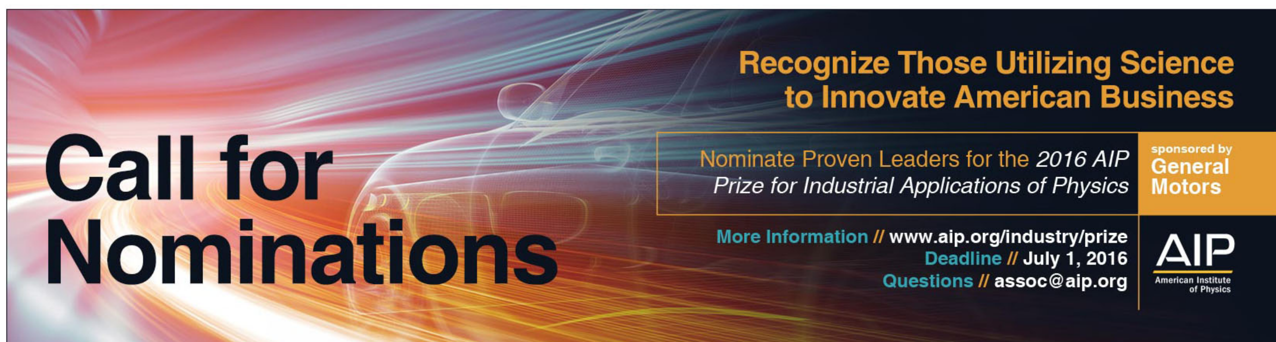

Reuse of AIP Publishing content is subject to the terms at: https://publishing.aip.org/authors/rights-and-permissions. Download to IP: 140.105.207.250 On: Fri, 13 May 2016 08:22:57

REVIEW OF SCIENTIFIC INSTRUMENTS **87**, 053703 (2016)

Operando x-ray photoelectron emission microscopy for studying forward and reverse biased silicon p-n junctions

N. Barrett,[1,a)] D. M. Gottlob,[1] C. Mathieu,[1] C. Lubin,[1] J. Passicousset,[1,2] O. Renault,[3] and E. Martinez[3]
[1]*SPEC, CEA, CNRS, Université Paris-Saclay, CEA Saclay, 91191 Gif-sur-Yvette Cedex, France*
[2]*IFP Energies nouvelles, Rond-point de l'échangeur de Solaize, BP 3, 69360 Solaize, France*
[3]*University Grenoble-Alpes, 38000 Grenoble, France and CEA, LETI, MINATEC Campus, 38054 Grenoble, France*

(Received 19 February 2016; accepted 21 April 2016; published online 9 May 2016)

Significant progress in the understanding of surfaces and interfaces of materials for new technologies requires operando studies, i.e., measurement of chemical, electronic, and magnetic properties under external stimulus (such as mechanical strain, optical illumination, or electric fields) applied *in situ* in order to approach real operating conditions. Electron microscopy attracts much interest, thanks to its ability to determine semiconductor doping at various scales in devices. Spectroscopic photoelectron emission microscopy (PEEM) is particularly powerful since it combines high spatial and energy resolution, allowing a comprehensive analysis of local work function, chemistry, and electronic structure using secondary, core level, and valence band electrons, respectively. Here we present the first operando spectroscopic PEEM study of a planar Si p-n junction under forward and reverse bias. The method can be used to characterize a vast range of materials at near device scales such as resistive oxides, conducting bridge memories and domain wall arrays in ferroelectrics photovoltaic devices. *Published by AIP Publishing.* [http://dx.doi.org/10.1063/1.4948597]

I. INTRODUCTION

Characterization of novel device architectures requires not only in depth knowledge of constituent material properties but also how they respond to applied bias. We would like to understand the electronic structure of the material underlying the observed capacitive, dielectric, magnetic, or transport properties of the device. Within this perspective, it is desirable to know how the electronic structure responds to external stimuli, i.e., operando experiments in as near as possible real operating conditions.

Atomic resolution can be provided by aberration-corrected transmission electron microscopy (TEM) and operando TEM is now reported.[1] However, sample preparation is extremely delicate, possibly modifying the very structure of interest and is, of course, destructive. Photoelectron spectroscopy provides non-destructive, surface sensitive, spectroscopic analysis, correlating chemical states with electronic energy levels. With this technique, surface and interface band bending,[2,3] oxide layer thickness,[4] surface photovoltage,[5] and valence band offsets[6] can all be measured simultaneously. Standard photoemission is an area-averaged technique but the characterization of realistic devices requires in addition suitable spatial resolution. Photoelectron spectromicroscopy, with spatial resolution of several tens of nanometers, goes some way to providing such a capability.

Scanning electron microscopy has been successfully used to analyze a planar silicon p-n junction.[7] Low energy emission microscopy (LEEM) provides information on the electron yield and doping levels across a p-n junction.[8] X-ray photoelectron emission microscopy (XPEEM) combines the high spectroscopic resolution of photoemission and the spatial resolution of electron microscopy[9] and has been successfully used for full field imaging of doped semiconductor microscopic patterns.[10–14] In this way the band bending and hence the depletion width of p-n junctions can be mapped making the technique ideal for the study of semiconductors in test device architectures.

The above studies have been done with a view to characterizing the band alignment as a function of chemistry, doping, and/or junction architecture. As yet, there have been no spatially resolved, spectroscopic studies of the response of the electronic structure of microscopic semiconductor patterns to *in situ* applied voltages.

Operando XPEEM measurements have been successfully carried out in absorption mode by measuring the secondary electron yield; see, for example, for time-resolved measurements magnetic domain switching following application of a current pulse.[15] However, in photoemission mode, operando measurements are quite challenging from a technical point of view because any change in the sample potential can modify the photoemission spectrum. Furthermore, the signals are usually much weaker than in absorption mode.

Simultaneously obtaining high spatial and spectroscopic resolution requires high photon flux, optimization of the photoionization cross section, and surface sensitivity, which can only be done using tunable photon sources. In general, such analysis is best carried out using synchrotron radiation although the intense light can also result in a significant surface photovoltage.[5] Here we report operando characterization of a

[a)]Author to whom correspondence should be addressed. Electronic mail: nick.barrett@cea.fr

Reuse of AIP Publishing content is subject to the terms at: https://publishing.aip.org/authors/rights-and-permissions. Download to IP: 140.105.207.250 On: Fri, 13 May 2016 08:22:57

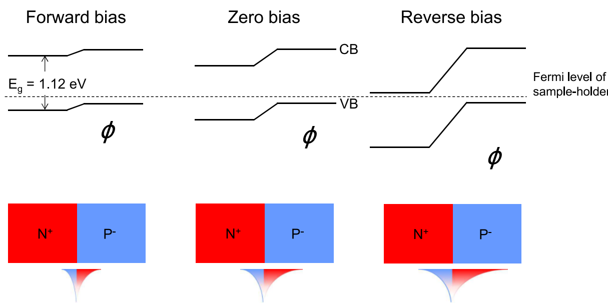

FIG. 1. Schematic band line-up at a p-n junction as a function of bias. The band gap is $E_g = 1.12$ eV. Going from forward to reverse bias, both the band offset and the depletion width increase. The operando band offset is given by $\phi = q(\Phi_{bi} - U_{bias})$, where Φ_{bi} is the zero field built-in potential and U_{bias} the applied bias.

planar Si p-n junction using energy filtered XPEEM in several *in situ* bias conditions. The well-known physics of the p-n junction provides an ideal test sample for the operando PEEM analysis. Due to the flat band offset, also called the built-in or diffusion potential, electrons diffuse from n type and holes from p type regions to become minority carriers in the p and n-type regions, respectively, setting up a region of space charge where drift and diffusion are balanced. The characteristic width of the depletion region is inversely proportional to the square root of the majority carrier concentration.[16] Both the band offset and the depletion width are modified in the presence of a bias voltage. In forward bias, the offset is reduced, allowing current to flow and the depletion width narrows, whereas in reverse bias the voltage step increases, blocking current flow. In this case, the depletion width becomes much broader. The expected behavior is illustrated schematically in Fig. 1 for forward, zero, and reverse bias.

As can be seen, when going from forward to reverse bias, both the band offset and the depletion width increase, becoming clearly greater than the zero field values for the case of reverse bias. As explained below, in our experiments, the p-doped region is at sample ground, hence the valence and conduction bands do not shift with bias voltage applied to the n-type region. The dotted line represents the Fermi level of the metallic sample holder which provides the reference for the electron energy.

In this paper, we report operando measurements of the band bending across the p-n junction using both threshold and core level imaging and confirm the expected rigid nature of the band shifts as a function of the applied *in situ* bias voltage. Both threshold and core level maps allow estimation of the depletion width and band alignment. The energy level alignment as a function of bias is in good qualitative agreement with that expected from basic semiconductor theory.

II. EXPERIMENT

The sample was made in the Laboratoire d'Electronique et de Technologie de l'Information (LETI) at the CEA-Grenoble. It consists of two-dimensional heavily doped n-type patterns implanted into a p-type silicon substrate. The nominal doping levels are 2.5×10^{19} cm^{-3} and 5.5×10^{15} cm^{-3} and the expected depletion widths are 6.4 nm and 0.43 μm in the n and p type regions, respectively.

The basic instrument is a second generation NanoESCA (ScientaOmicron) and comprises a fully electrostatic PEEM column, followed by an imaging double energy analyzer, as an energy filter. The best spatial resolution is 30 nm whereas the best energy resolution in spectroscopic threshold PEEM, measured at low temperature (35 K), is 28 meV. The high precision, 4-axis sample stage allows *in situ* application of bias voltages up to ±100 V by means of two contacts inside the PEEM sample holder, insulated from the sample-holder by ceramic tubes, see picture in Figs. 2(a) and 2(b).

The sample is wired from inside the sample-holder. The bias pins are automatically contacted to UHV feedthroughs when the sample-holder is inserted into the manipulator. Figure 2 shows a schematic of sample wiring allowing application of U_{bias} on only a chosen n-type region. The

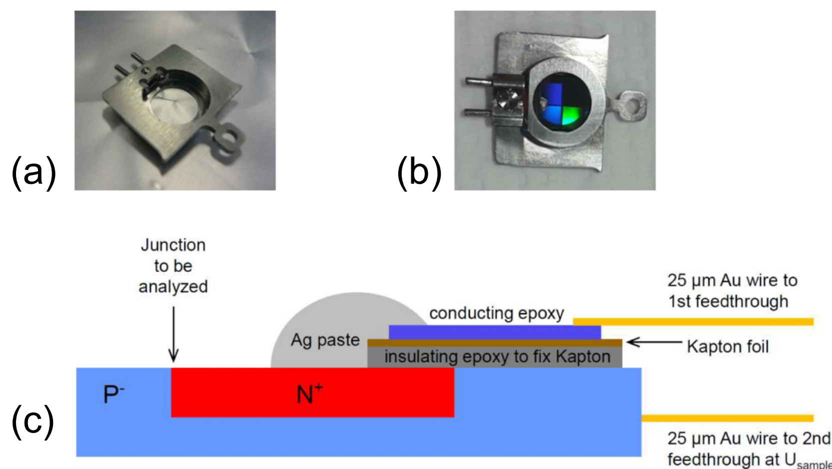

FIG. 2. (a) Photograph of sample-holder from below showing contact pins for application *in situ* of bias voltages. The sample is wired from inside the sample-holder; the bias pins are automatically contacted to UHV feedthroughs when the sample-holder is inserted into the manipulator. (b) Sample mounted is in sample-holder; the colored squares allow for optical recognition of doping regions. (c) Schematic of sample wiring allowing application of U_{bias} on only a chosen n-type region. The p-type region is at the sample-holder potential. Two 25 μm Au wires cable the n and p-type regions to the electrical feedthroughs visible in Fig. 2. An additional kapton washer isolates the sample surface from the sample-holder, allowing the lower Au wire to connect only the p-type region to U_{sample}.

Reuse of AIP Publishing content is subject to the terms at: https://publishing.aip.org/authors/rights-and-permissions. Download to IP: 140.105.207.250 On: Fri, 13 May 2016 08:22:57

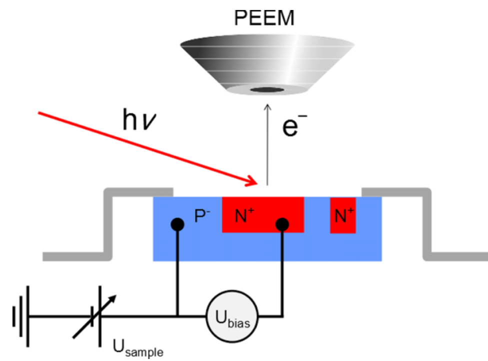

FIG. 3. Schematic cross section of sample mounting. U_{bias} allows biasing of the p-n junction by application of U_{bias} to a particular n-type pattern, whilst the reference potential, U_{sample}, is maintained on the p-type sample substrate. Other n-type patterns are either at zero bias or floating potential.

p-type region is held at the sample-holder potential. Two 25 μm Au wires cable the n and p-type regions to the electrical feedthroughs visible in Figure 2. An additional kapton washer isolates the sample surface from the sample-holder, allowing the lower Au wire to connect only the p-type region to U_{sample}.

Figure 3 shows a schematic of the sample geometry and basic wiring allowing application of bias across a particular p-n junction during photoemission spectromicroscopic measurements. The junctions were imaged within a field of view (FoV) of 88 μm. The photon energy was 127 eV, the overall energy resolution (beamline and analyzer) was 0.2 eV. All measurements were done at room temperature.

Bias voltages of ±1.5 V were applied to one n-type region with respect to the p-type substrate in the microscope FoV. Image series of the biased p-n junction were acquired at photoemission threshold and the Si 2*p* core levels. An energy step of 25 meV was used for the threshold spectra. All measurements were carried out at room temperature. Note that the photoelectron energy is measured with respect to the Fermi level (E_F) of the sample holder. Thus, the work function is the value of E-E_F for the photoemission threshold.

Images were corrected for detector inhomogeneity by a flat field obtained from a uniform part of the sample. Any spatial variation in the intensity of the flat field is due to the detector.[14] The vertical direction in the images is the dispersion direction of the energy analyzer. The energy dispersion, called non-isochromaticity, is parabolic and depends on the pass energy, the analyzer slits, and the FoV.[17] It is worthwhile noting that sample is part of the system; therefore, after alignment of the microscope, the optical axis is in the center of the field of view. In this configuration, any electron coming from any other position (i.e., off-axis points) with the same take-off angle is transferred by the coupling lenses to electron paths inside the PEEM optics with larger angles. For a point on the sample off-axis in the dispersive direction, the energy shift varies with the square of the distance from the optical axis. The threshold image series have been corrected for this non-isochromaticity and for detector inhomogeneity. Finally, the work function maps were obtained from a pixel-by-pixel error function fit to the rising edge of the threshold spectra.

III. RESULTS AND DISCUSSION

Figure 4(a) is a sketch of the planar p-n structure, the p-type substrate is gray, and the heavily n-doped patterns (N^+) are white. The red circle highlights the 88 μm FoV. Thus, the vertical N^+ line can be biased whereas the N^+ structure on the right hand side of the FoV is floating. Figures 4(b) and 4(c) show threshold images, taken at E-E_F = 2.7 and 4.0 eV for the reverse biased p-n junction. Reverse bias is chosen since it provides the best illustration of contrast inversion due to work function variation with doping. At the lower E-E_F value, photoemission is observed only from the N^+ region, indicating that the work function is smaller than for the P type substrate. As E-E_F increases, the surrounding p-type region also contributes and, as shown in Fig. 4, becomes more intense than the photoemission from the n-type region. The contrast inversion is a clear signature of band offset. In Fig. 4(c) a third region, labeled "N^+ floating," is visible with intermediate intensity between that of N^+ and P^-. This triple contrast has been explained in a previous paper.[11] The region corresponds to the enclosed N^+ pattern in the p-type in Fig. 4(a) and, as can be seen from Figure 2(b), is not connected to U_{bias}. In the following, we focus on the p-n junction formed by the N^+ and P^- patterns wired to the bias voltage.

In Figure 5 we show the threshold spectra extracted from N^+ and P^- regions for forward and reverse biased (±1.5 V) p-n

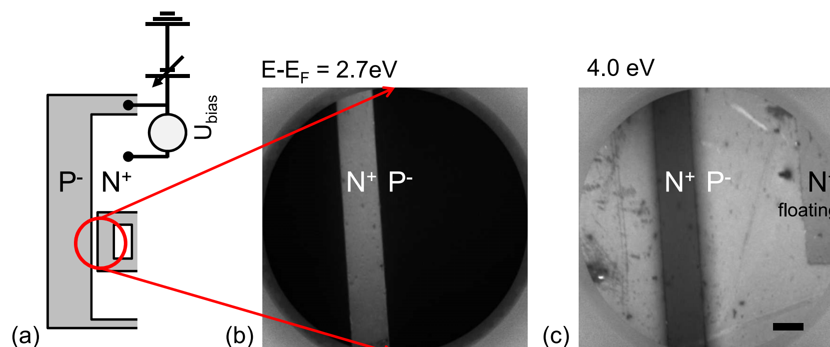

FIG. 4. (a) Schematic of p-n patterns. The FoV of the PEEM is indicated by the red circle. Note that only the larger, open N^+ pattern is wired to U_{bias}. The smaller N^+ pattern at the right hand side of the FoV is at floating potential. Energy-filtered threshold images of reverse biased sample (+1.5 V on N^+ pattern) for (b) 2.7 eV and (c) 4.0 eV values of E-E_F, showing clear contrast inversion due to local work function differences. The scale bar is 10 μm.

Reuse of AIP Publishing content is subject to the terms at: https://publishing.aip.org/authors/rights-and-permissions. Download to IP: 140.105.207.250 On: Fri, 13 May 2016 08:22:57

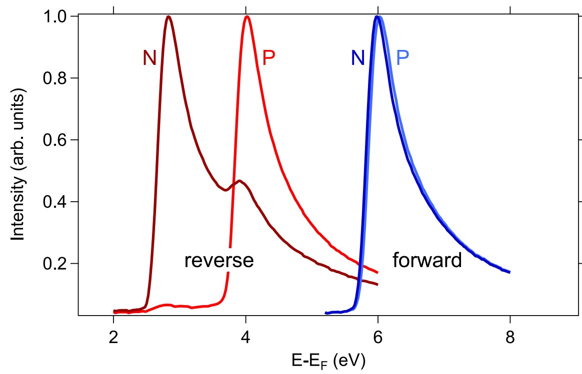

FIG. 5. Photoemission threshold spectra extracted from 8×8 μm^2 regions of N^+ and P^- patterns for forward (blue) and reverse (red) bias (±1.5 V). The threshold spectra from the N and P patterns are shifted by 1.2 eV at reverse bias.

junctions. It can be seen that the threshold spectra are almost superimposed on each other in forward bias whereas they are shifted by 1.2 eV at reverse bias, qualitatively consistent with the expected band alignments sketched in Fig. 1. In addition to the main peak, there is an additional structure in the reverse bias threshold spectra from the N and P type patterns at 3.9 and 2.8 eV, respectively, i.e., at the maxima of the P and N secondary electron emission. This is because the image is formed by electrons impinging on a screen generating light recorded by the camera. Scattered light from outwith the region of interest (N or P) between the screen and the camera creates an intensity artefact in the image series. It is much stronger in the N type spectrum simply because the P pattern occupies most of the field of view, hence the scattered intensity is stronger; however, it does not affect the value of the work function which is given by the main leading edge.

Since the photoemission threshold measured on the scale of E-E$_F$ is strictly equivalent to the sample work function, we can use the threshold image series to map the local work function across the whole field of view. Using an automatic procedure on the 161 image stack, the rising edge of the photoemission signal is extracted from each of the 600×600 pixels and fitted using an error function.

The resulting work function maps are shown in Fig. 6 for (a) forward, (b) zero, and (c) reverse bias. Note that the color code dynamic of the work function scale is the same in each case, showing the clear contrast enhancement in the case of reverse bias with respect to or forward bias. The scale E-E$_F$

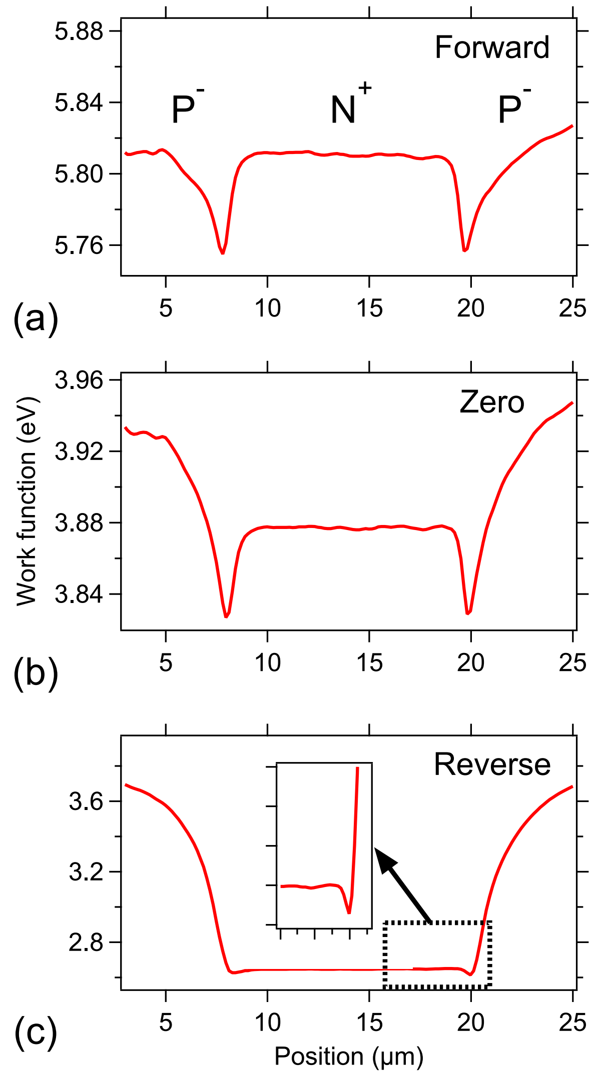

FIG. 7. Variation in local work function across $P^-/N^+/P^-$ outlined by the dotted rectangle in Fig. 6(a) at (a) forward, (b) zero, and (c) reverse bias.

is also shifted by the bias voltage (±1.5 V) which adds to the sample bias.

At zero bias, there is a band offset of ∼0.1 eV between the N^+ and P^- regions. The offset almost disappears under forward bias but becomes much stronger (1.2 eV) in reverse bias, as can be seen from Fig. 6(c). In each case, the floating enclosed N^+ region has a different work function due to uncompensated charging during photoemission.[11] The measured band line-ups

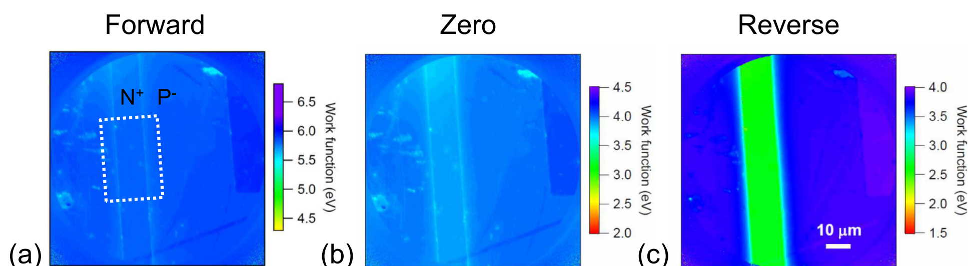

FIG. 6. Work function maps obtained from a pixel by pixel fit across the 88 μm FoV at (a) forward, (b) zero, and (c) reverse bias. In each case, the color range spans 2.5 eV, shifted only by the applied bias, U_{bias}. The p-n band offset is 0.01 eV, 0.10 eV, and 1.20 eV for forward, zero, and reverse bias conditions, respectively. The dotted line in (a) indicates the area used to extract the WF profile across the P^--N^+-P^- structure in Fig. 7.

Reuse of AIP Publishing content is subject to the terms at: https://publishing.aip.org/authors/rights-and-permissions. Download to IP: 140.105.207.250 On: Fri, 13 May 2016 08:22:57

are therefore in qualitative agreement with expected values. However, there are quantitative differences which need to be addressed. As can be seen in Fig. 6(b), the work function values at zero bias differ by 0.1 eV and not 0.87 eV as one would expect from the nominal p and n type doping and the intrinsic carrier concentration. There are two possible reasons for this. First, the surface photovoltage which tends to reduce band bending and second, it should be remembered that the signal comes mainly from the oxide overlayer and not the underlying n or p type silicon. The surface band bending will therefore be modified, giving, at zero bias an offset $V_{offset} = 0.1 - U_{bi} = -0.77$. The thin chemical oxide layer introduces band bending at the oxide/silicon interface which tends to equalize or at least reduce the difference in band offsets between p and n type regions, observed in forward bias and reverse bias. In reverse bias the measured band offset is 1.20 eV, also considerably smaller than the expected value given by $q(\Phi_{bi} - U_{bias}) = 2.37$ eV. This again suggests that E_F might be pinned by oxide/substrate defects. Using the estimation of $V_{offset} = -0.77$ V at zero bias, we would expect a band offset of 1.6 eV which is not far from the experimental value of 1.2 eV.

The difference between the bottom of the conduction band and the vacuum level is the electron affinity and is chemistry dependent. Assuming that the extreme surface chemistry does not vary between p- and n-type patterns (it is a chemical SiO_2 oxide), then the electron affinity is constant. As a result, the work function can be used as local measurement of the relative conduction and valence band positions. The profile across the p-n junction map therefore provides a direct trace of band bending and hence an estimation of the depletion width. Figure 7 shows the variation in the local work function across the P^--N^+-P^- structure, at (a) forward, (b) zero, and (c) reverse bias. There is a dip in intensity near each p-n junction which we attribute to the stray built-in field. Comparison with simulations of the effect of the stray field from the built-in potential on the electron paths would be necessary to precisely locate the position of the physical junction.[18] The inset of Figure 7(c) shows the same form of intensity profile across the reverse biased junction as in forward and zero bias conditions.

The depletion region extends mainly into the P type pattern as expected from the relative p and n doping levels. Far from the junction, the bands are almost aligned for forward bias, as expected whereas for reverse bias, the misalignment is greater than 1 eV. The flat band regime is reached in a fraction of a micron on the N^+ side of the junction whereas the band bending extends several microns on the P^- side. This is in good agreement with the relative, nominal p and n doping levels which would lead one to expect a difference of a factor 70 in the depletion widths. The apparent depletion width in the heavily doped N pattern is given by the lateral resolution of 100 nm, much greater than the expected depletion width of 6.4 nm. This explains the discrepancy in the ratio of the space charge regions measured on either side of the junction.

The higher kinetic energy of the Si 2*p* spectra means that the effect of the in-plane built-in potential on the electron trajectories becomes negligible[18] and therefore might provide the most reliable measurement of band bending. The local Si 2*p* core level spectra rigidly follow the band shift at the p-n

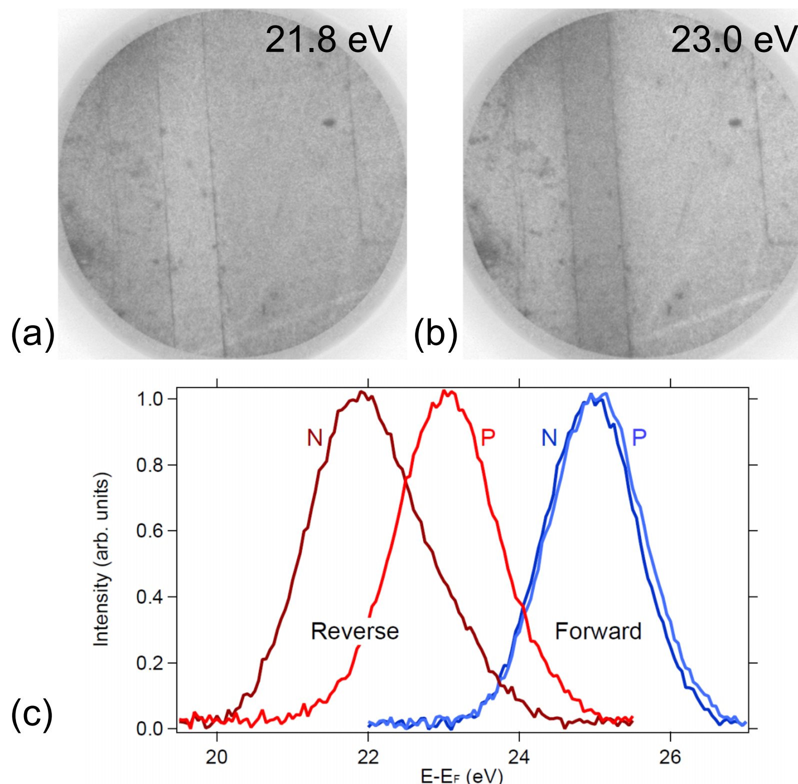

FIG. 8. Images taken at maximum intensity of Si 2*p* from the (a) N^+ and (b) P^- regions for reverse biased sample showing clearly the contrast inversion in the core level emission. (c) Core level spectra extracted from N^+ and P^- regions for forward (blue) and reverse (red) biased (±1.5 V) samples.

Reuse of AIP Publishing content is subject to the terms at: https://publishing.aip.org/authors/rights-and-permissions. Download to IP: 140.105.207.250 On: Fri, 13 May 2016 08:22:57

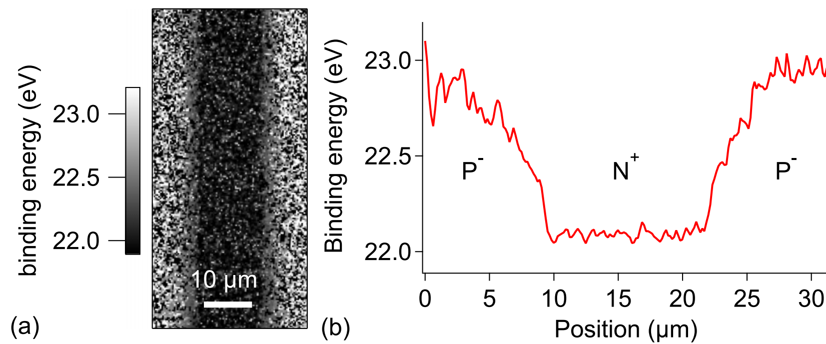

FIG. 9. (a) Pixel-by-pixel fit across the FoV of the Si 2*p* emission. Scale bar is 10 μm. (b) Band bending across back-to-back p-n junctions extracted from the fit in (a) integrated over the full image.

junction deduced from the work function analysis. Figure 8 shows images taken at maximum intensity of Si 2*p* from the (a) N^+ and (b) P^- regions for reverse biased sample. There is clear contrast inversion in the core level emission from the two regions which is the signature of band offset. Figure 8(c) shows the Si 2*p* spectra extracted from N^+ and P^- regions for forward (blue) and reverse (red) biased (±1.5 V) samples. The local spectra have been background subtracted using a polynomial function. Whereas under forward bias the 2*p* spectra are virtually superimposed, under reverse bias there is a ∼1.2 eV shift, exactly like the threshold spectra.

A first analysis of the band bending as determined from the Si core level emission is shown in Fig. 9 for the reverse biased P^--N^+-P^-. A pixel-by-pixel fit to Si 2*p* emission across the full FoV has been carried out, giving a map of the Si 2*p* binding energy, shown in Fig. 9(a). Fig. 9(b) shows the binding energy profile across the y-averaged map of Fig. 9(a). As can be seen, the depletion region extends much further on the P^- side of the junction than on the N^+ side. However, like the work function profiles shown in Fig. 7, the size of the depletion region is greater than that expected from semiconductor theory. One reason for the discrepancy may be due to the lateral resolution of the PEEM. Another may be quite simply the rather low statistics of the core level emission. Finally, the presence of stay lateral fields can influence the apparent depletion width.[18]

The results show that in principle it should be possible to extract true band bending operando from planar semiconductor structures such as the model p-n junction studied here. However, this requires careful attention to surface cleanliness which might otherwise pin electronic levels and effects such as the surface photo-voltage which can naturally countervail band bending when using the more intense synchrotron radiation.

Looking further ahead, it would be interesting to conduct a series of experiments on local work function modulation of, for example, photocathode material or for *in situ* studies of optoelectronic devices.

IV. CONCLUSION

We have used energy-filtered photoelectron emission microscopy to study the electronic band structure across a silicon p-n junction as a function of applied bias. A dedicated sample-holder allowed application of zero, forward, and reverse bias voltages *in situ* during the experiment and provides proof of principle results of operando photoemission-based PEEM. Synchrotron radiation was used to probe both photoemission threshold and the Si 2*p* core levels. The characteristic band lineup of a p-n junction is observed and is in qualitative agreement with the expected values. Work function and core level shifts across the p-n junction can be used to estimate the depletion width. More quantitative agreement could be achieved by taking into account the band bending at the silicon/oxide interface. The method can be applied to a wide range of samples containing microscopic structures suitable for electronics applications such as nanostripes and ribbons, ferroelectric domains, and resistive oxides.

ACKNOWLEDGMENTS

We thank Nicola Zema, Stefano Turchini, Daniele Catone, Sandro Rinaldi, and Michael Kallmayer for invaluable technical assistance. We gratefully acknowledge Elettra for the provision of synchrotron radiation facilities. D.G. was funded by the CEA Operando+ project. J.P. was supported by the Agence National de la Recherche Project No. ANR-12-IS04-0001-01 CHEM-SWITCH.

[1]A. Marchewka, D. Cooper, C. Lenser, S. Menzel, H. Du, R. Dittmann, R. E. Dunin-Borkowski, and R. Waser, Sci. Rep. **4**, 6975 (2014).
[2]S. Sayan, T. Emge, E. Garfunkel, X. Zhao, L. Wielunski, R. a. Bartynski, D. Vanderbilt, J. S. Suehle, S. Suzer, and M. Banaszak-Holl, J. Appl. Phys. **96**, 7485 (2004).
[3]L. Q. Zhu, N. Barrett, P. Jegou, F. Martin, C. Leroux, E. Martinez, H. Grampeix, O. Renault, and A. Chabli, J. Appl. Phys. **105**, 024102 (2009).
[4]F. Himpsel, F. McFeely, A. Taleb-Ibrahimi, J. Yarmoff, and G. Hollinger, Phys. Rev. B **38**, 6084 (1988).
[5]M. Marsi, L. Nahon, M. Couprie, D. Garzella, T. Hara, R. Bakker, M. Billardon, A. Delboulbe, G. Indlekofer, and A. Taleb-Ibrahimi, J. Electron Spectrosc. Relat. Phenom. **94**, 149 (1998).
[6]N. Barrett, O. Renault, J. F. Damlencourt, and F. Martin, J. Appl. Phys. **96**, 6362 (2004).
[7]R. J. Phaneuf, H.-C. Kan, M. Marsi, L. Gregoratti, S. Günther, and M. Kiskinova, J. Appl. Phys. **88**, 863 (2000).
[8]L. Frank, I. Müllerová, D. A. Valdaitsev, A. Gloskovskii, S. A. Nepijko, H.-J. Elmers, and G. Schönhense, J. Appl. Phys. **100**, 093712 (2006).

Reuse of AIP Publishing content is subject to the terms at: https://publishing.aip.org/authors/rights-and-permissions. Download to IP: 140.105.207.250 On: Fri, 13 May 2016 08:22:57

[9]O. Renault, N. Barrett, A. Bailly, L. F. Zagonel, D. Mariolle, J. C. Cezar, N. B. Brookes, K. Winkler, B. Krömker, and D. Funnemann, Surf. Sci. **601**, 4727 (2007).
[10]S. Günther, B. Kaulich, L. Gregoratti, and M. Kiskinova, Prog. Surf. Sci. **70**, 187 (2002).
[11]M. Lavayssière, O. Renault, D. Mariolle, M. Veillerot, J. P. Barnes, J. M. Hartmann, J. Leroy, and N. Barrett, Appl. Phys. Lett. **99**, 202107 (2011).
[12]N. Barrett, L. F. Zagonel, O. Renault, and A. Bailly, J. Phys.: Condens. Matter **21**, 314015 (2009).
[13]O. Renault, M. Lavayssière, A. Bailly, D. Mariolle, and N. Barrett, J. Electron Spectrosc. Relat. Phenom. **171**, 68 (2009).
[14]F. de la Peña, N. Barrett, L. Zagonel, M. Walls, and O. Renault, Surf. Sci. **604**, 1628 (2010).
[15]A. Krasyuk, F. Wegelin, S. A. Nepijko, H. J. Elmers, G. Schönhense, M. Bolte, and C. M. Schneider, Phys. Rev. Lett. **95**, 1 (2005).
[16]S. M. Sze and K. K. Ng, *Physics of Semiconductor Devices* (John Wiley & Sons, 2006).
[17]M. Escher, K. Winkler, O. Renault, and N. Barrett, J. Electron Spectrosc. Relat. Phenom. **178-179**, 303 (2010).
[18]M. Lavayssière, M. Escher, O. Renault, D. Mariolle, and N. Barrett, J. Electron Spectrosc. Relat. Phenom. **186**, 30 (2013).

Reuse of AIP Publishing content is subject to the terms at: https://publishing.aip.org/authors/rights-and-permissions. Download to IP: 140.105.207.250 On: Fri, 13 May 2016 08:22:57